Geophysical Research Letters

Supporting Information for

Spatial representativeness error in the ground-level observation networks for black carbon radiation absorption

Rong Wang[a,b,d,*], Elisabeth Andrews[c], Yves Balkanski[d], Olivier Boucher[e], Gunnar Myhre[f], Bjørn Hallvard Samset[f], Michael Schulz[g], Gregory L. Schuster[h], Myrto Valari[i], Shu Tao[j]

[a]Department of Environmental Science and Engineering, Fudan University, Shanghai 200433, China; [b]Department of Global Ecology, Carnegie Institution for Science, Stanford, California 94305, USA; [c]CIRES, University of Colorado, Boulder, Colorado 80309, USA; [d]Laboratoire des Sciences du Climat et de l'Environnement, CEA CNRS UVSQ, Gif-sur-Yvette 91191, France ; [e]Institut Pierre-Simon Laplace, CNRS / Université Pierre et Marie Curie, Paris Cedex 75252, France ; [f]CICERO Center for International Climate and Environmental Research, Oslo 0318, Norway; [g]Norwegian Meteorological Institute, Oslo 0313, Norway; [h]NASA Langley Research Center, Hampton, Virginia 23681, USA; [i]Laboratoire de Météorologie Dynamique, IPSL/CNRS, Ecole Polytechnique, Palaiseau Cedex 91128, France ; [j]Laboratory for Earth Surface Processes, College of Urban and Environmental Sciences, Peking University, Beijing 100871, China.

Contents of this file

Figures S1 to S9

Additional Supporting Information

Supporting Spreadsheet

* Corresponding author

Email: rongwang@fudan.edu.cn

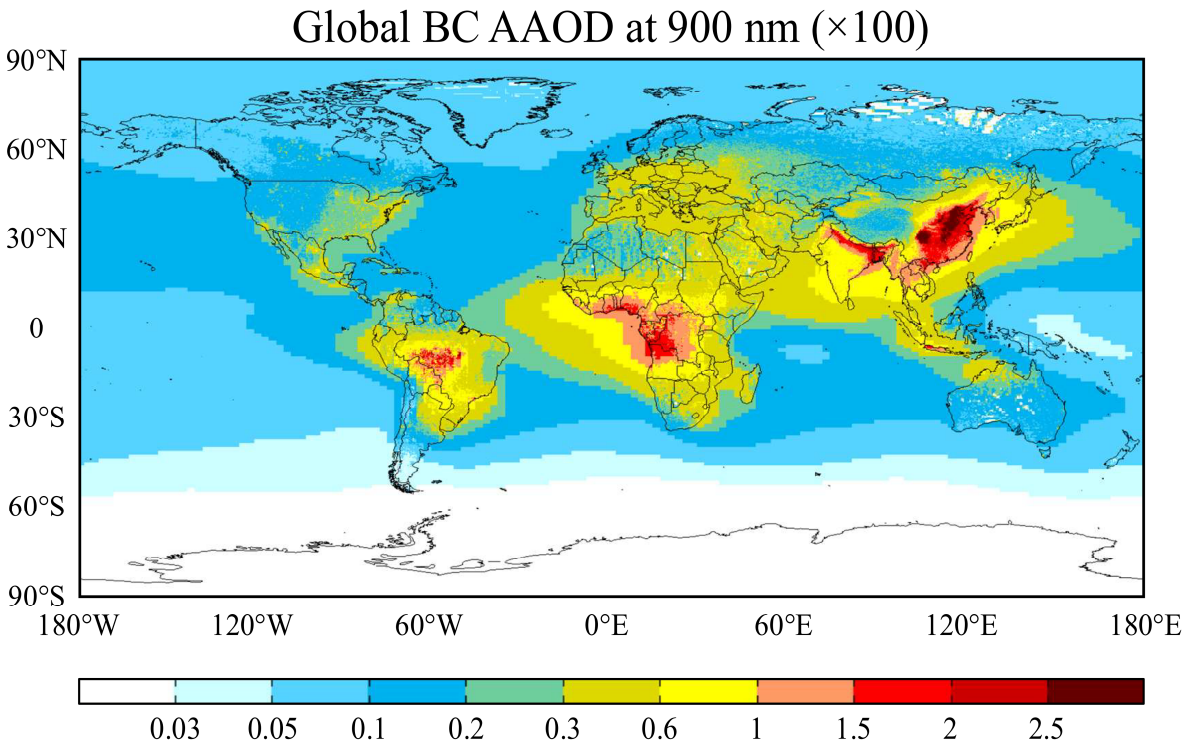

Figure S1. Global distribution of BC aerosol absorption optical depth (AAOD) at 900 nm downscaled to a horizontal resolution of 0.1°×0.1° in 2007.

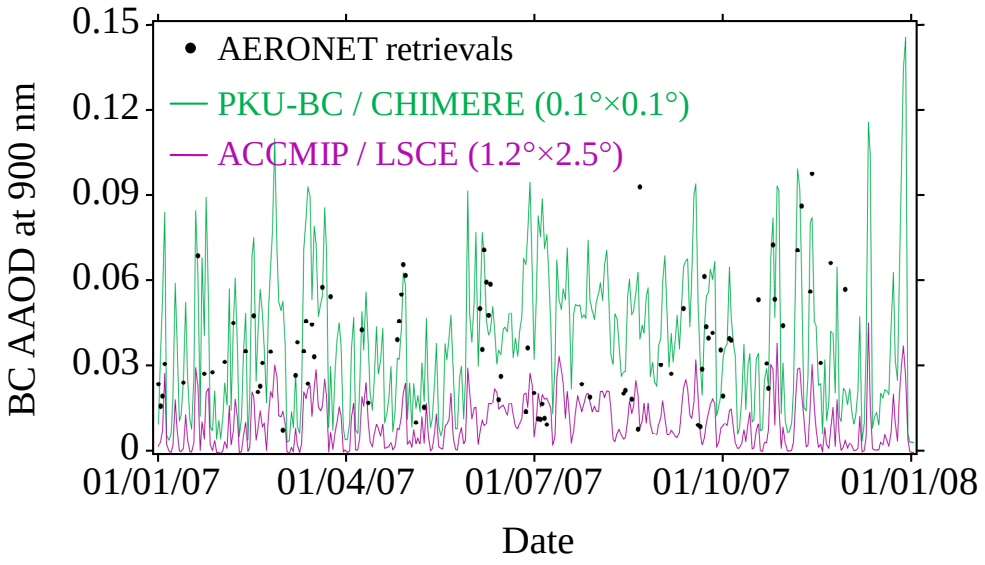

Figure S2. Comparison of retrieved (black dots) and modeled BC AAOD at Beijing. The purple line denotes BC AAOD modeled by a global coarse-resolution aerosol climate model, LMDZ-OR-INCA (Schulz *et al.*, 2006), at a resolution of 1.2°×2.5° driven by a country-level emission inventory, ACCMIP (Lamarque *et al.*, 2010). The green line denotes BC AAOD modeled by a regional chemical transport model at a resolution of 0.1°×0.1°, CHIMERE (Menut et al., 2013), driven by a county-level emission inventory, PKU-BC (Wang et al., 2014).

References:

Lamarque, J. F. *et al.* Historical (1850-2000) gridded anthropogenic and biomass burning emissions of reactive gases and aerosols: Methodology and application. *Atmos. Chem. Phys.* **10**, 7017-7039 (2010).

Menut, L. *et al.* CHIMERE 2013: a model for regional atmospheric composition modeling. *Geosci. Model Dev.* **6**, 981-1028 (2013).

Schulz, M. *et al.* Radiative forcing by aerosols as derived from the AeroCom present-day and pre-industrial simulations. *Atmos. Chem. Phys.* **6**, 5225-5246 (2006).

Wang, R. *et al.* Exposure to ambient black carbon derived from a unique inventory and high - resolution model. *Proc. Natl. Acad. Sci. U. S. A.* **111**, 2459-2463 (2014).

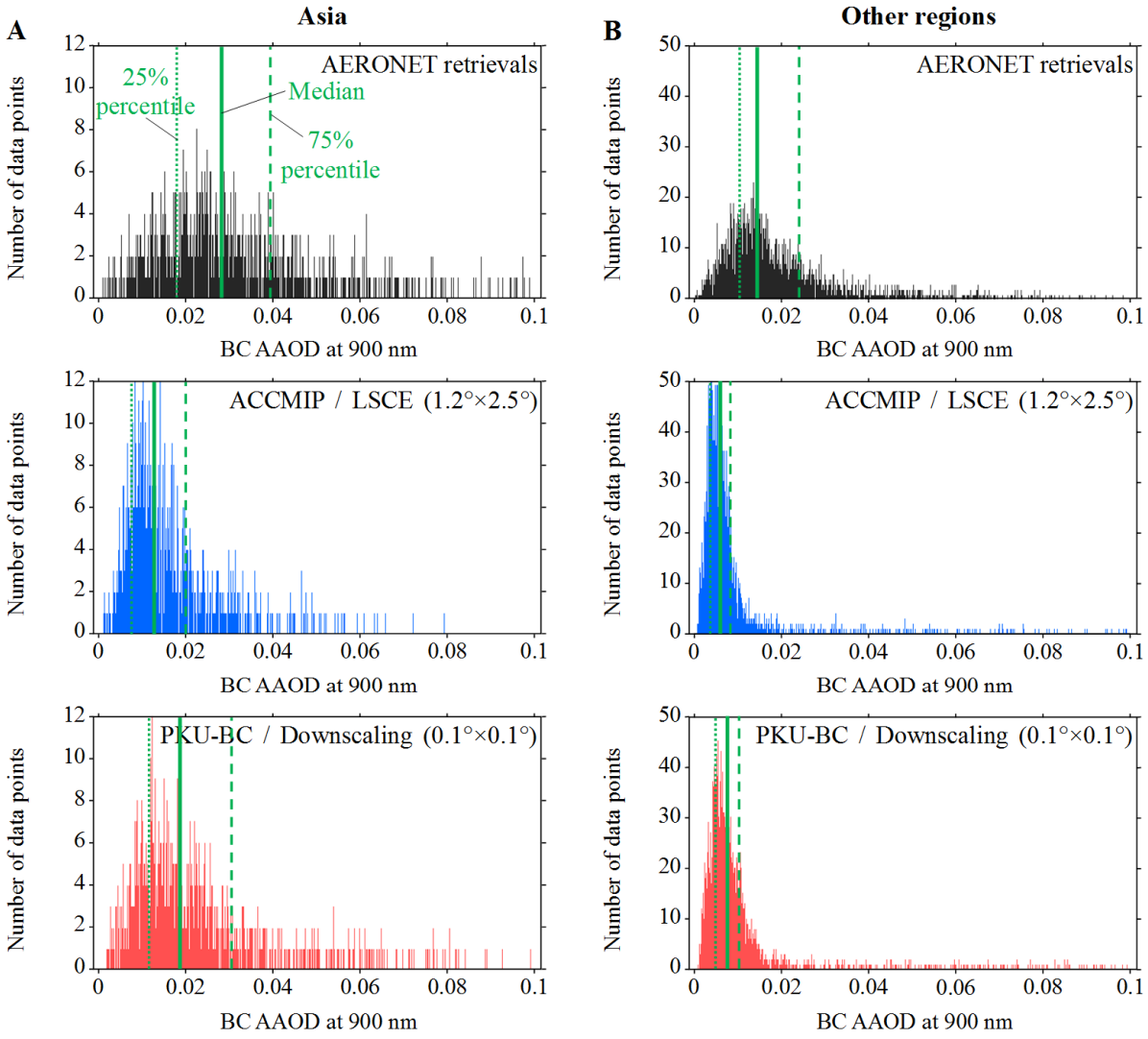

Figure S3. Comparison of the frequency distribution of retrieved and modeled BC AAOD at AERONET sites for year 2007 for sites (**A**) in Asia and (**B**) in other regions. The black bars (top) show the frequency distributions of BC AAOD retrieved from AERONET observations. The blue bars (middle) show the frequency distributions of BC AAOD at these sites modeled by a global aerosol climate model, LMDZ-OR-INCA (Schulz *et al.*, 2006), at a resolution of 1.2°×2.5° driven by a low-resolution version of emission inventory, ACCMIP (Lamarque *et al.*, 2010). The red bars (bottom) show the frequency distributions of BC AAOD at these sites from the 0.1°×0.1° map in **Figure S1**, constructed by using a high-resolution emission inventory PKU-BC (Wang *et al.*, 2014) and a downscaling method. The green lines show the median (solid line) as well as the 25% (dotted line) and 75% (dashed line) percentiles. The frequency is computed at a BC-AAOD interval of 0.0001.

References:

Lamarque, J. F. *et al.* Historical (1850-2000) gridded anthropogenic and biomass burning emissions of reactive gases and aerosols: Methodology and application. *Atmos. Chem. Phys.* **10**, 7017-7039 (2010).

Schulz, M. *et al.* Radiative forcing by aerosols as derived from the AeroCom present-day and pre-industrial simulations. *Atmos. Chem. Phys.* **6**, 5225-5246 (2006).
Wang, R. *et al.* Exposure to ambient black carbon derived from a unique inventory and high resolution model. *Proc. Natl. Acad. Sci. U. S. A.* **111**, 2459-2463 (2014).

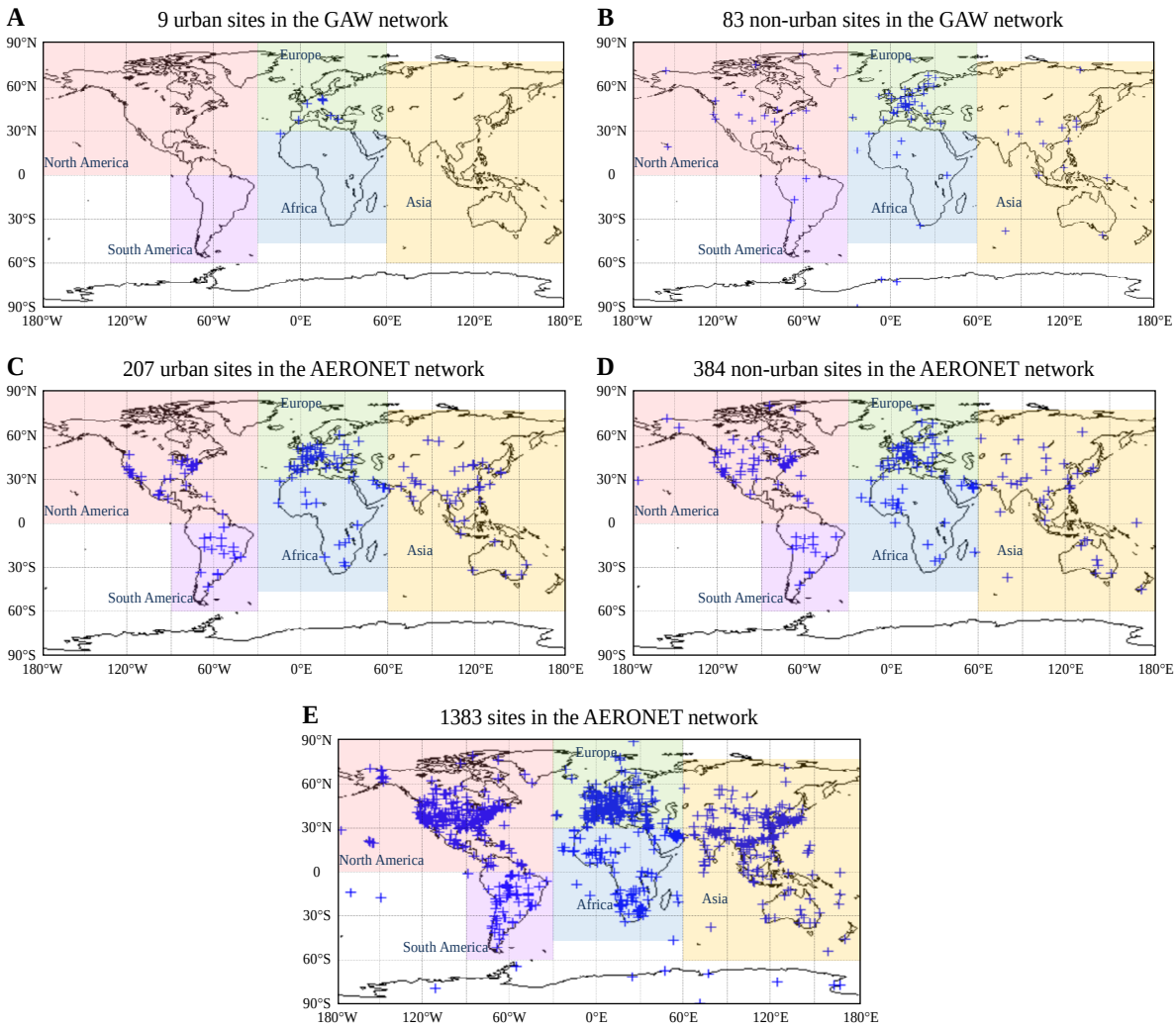

Figure S4. Geographical distributions of sites with absorbing aerosol observations in the GAW (**A**-**B**) and AERONET (**C**-**E**) networks. The GAW network (WMO, 2016) includes 9 urban sites (**A**) and 83 non-urban (**B**) sites, among which there are 11 sites in polar regions, 60 sites in continental regions, and 21 sites in coastal / marine regions. For AERONET (Holben *et al.*, 1998; Dubovik and King, 2000), we compiled data at 591 sites in 2013, which are identified as urban and non-urban sites. Among these 591 sites, we identified that there are 207 urban sites (**C**) and 384 non-urban (**D**) sites, among which there are 15 sites in polar regions, 442 sites in continental regions, and 134 sites in coastal / marine regions. It should be noted that the AERONET network has been extended to 1383 sites in 2017 (https://aeronet.gsfc.nasa.gov/), shown in (**E**). We use the 591 sites in **C**,**D** in our baseline calculation of the representativeness error, which is compared to that in a sensitivity case by using the 1383 sites in **E**.

References:

Dubovik, O. & King, M. A flexible inversion algorithm for retrieval of aerosol optical properties from sun and sky radiance measurements. *J. Geophy. Res. Atmos.* **105**, 20673-20696 (2000).

Holben, B. N. *et al.* AERONET - A federated instrument network and data archive for aerosol characterization. *Remote Sens. Environ.* **66**, 1-16 (1998).
WMO, 2016. *WMO/GAW Aerosol Measurement Procedures, Guidelines, and Recommendations*, WMO TD No. 1177, GAW Report No. 227, World Meteorological Organization, Geneva, Switzerland. Available at: https://library.wmo.int/opac/doc_num.php?explnum_id=3073

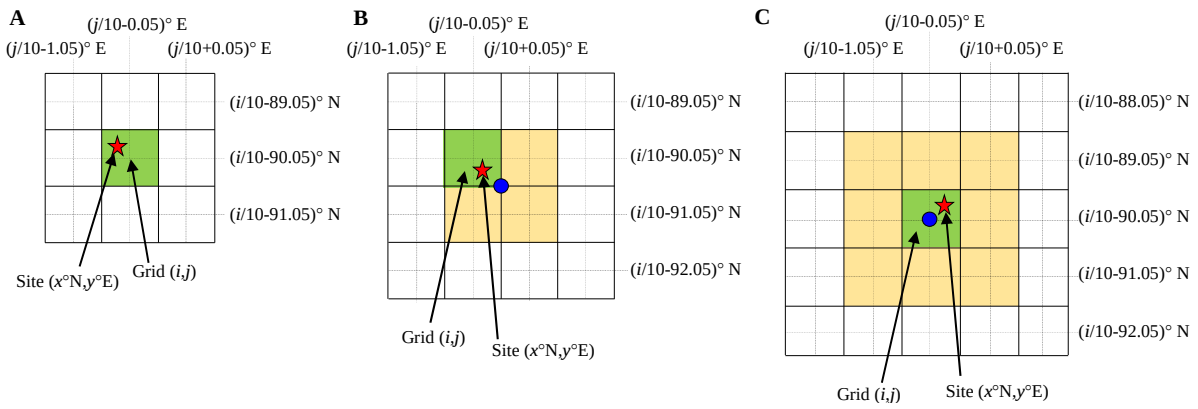

Figure S5. A schematic map of calculating BC AAOD for a 0.1°×0.1° grid or for a g°×g° grid, in which the monitoring site is closest to the center. A 0.1°×0.1° grid (i,j) is defined with a geographical center at (i/10-90.05)° N and (j/10-0.05)° E, where the ranges for i and j are $1 \le i \le 1800$ and $1 \le j \le 3600$. (**A**) When using a 0.1°×0.1° grid to represent a local site (x° N, y° E), we determine the 0.1°×0.1° grid using the conditions: (i/10-90)≤x≤(i/10-89) and (j/10-1)≤y≤j/10, shown as the green box. C_{fine} is calculated as the BC AAOD modeled for this green grid. (**B**) When using a 0.2°×0.2° coarse grid to represent a local site, we firstly determine the 0.1°×0.1° grid (green box) using the same conditions as above. Then, of the four vertices of the 0.1°×0.1° grid, we use the one with the shortest distance to the site as the center (blue circle) to construct a 0.2°×0.2° grid composed of four 0.1°×0.1° grids (the green box plus the three yellow boxes), which is used to represent the site. Similar approaches are applied when using a 0.4°×0.4°, 0.6°×0.6°, 0.8°×0.8°, … coarse grid (even multipliers of the 0.1° grid) to represent a local site. C_{coarse} for g=0.2, 0.4, 0.6, 0.8, … is calculated as the BC AAOD modeled averaged for these 0.1°×0.1° grids. (**C**) When using a 0.3°×0.3° coarse grid to represent a local site, we firstly determine the 0.1°×0.1° grid (green box) using the same conditions as (**B**). Then, we use the center of the 0.1°×0.1° grid as the center (blue circle) to construct a 0.3°×0.3° grid composed of nine 0.1°×0.1° grids (the green box plus the yellow boxes), which is used to represent the site. Similar approaches are applied when using a 0.5°×0.5°, 0.7°×0.7°, 0.9°×0.9°, … coarse grid to represent a local site (odd multipliers of the 0.1° grid). C_{coarse} for g=0.3, 0.5, 0.7, 0.9, … is calculated as the BC AAOD modeled averaged for these 0.1°×0.1° grids. It should be noted that there is a caveat in our method in (**A**-**C**). Our model is unable to distinguish the difference of two sites if they are located very close to each other, because we are dividing the globe into 0.1°×0.1° grids (*e.g.*, at a spatial scale of ~10 km× ~10 km in the equator). For example, for two sites locating with a distance of only 1.5 km, if they are located in the two neighboring 0.1°×0.1° grids, they will be located in two 0.1°×0.1° grids, of which the distance between the two grid centers is 10 km.

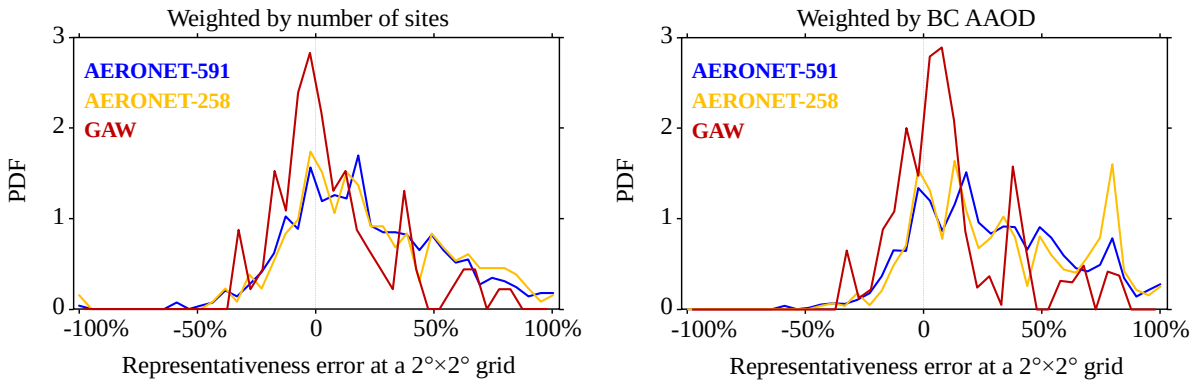

Figure S6. Probability density function (PDF) distribution of the representativeness error (*RE*) using BC AAOD over a 2°×2° grid-box relative to a 0.1°×0.1° resolution positioned at GAW (red) and AERONET (blue or orange) sites. The left panel shows the distribution weighted by the number of sites, and the right panel shows the distribution weighted by the modeled BC AAOD. For AERONET, we compare the result by using 591 sites (blue) covering data up to 2013 by Wang *et al.* [2016] or 258 sites (orange) covering data up to 2008 by Kinne *et al.* [2013].

References:

Wang, R., *et al.* (2016), Estimation of global black carbon direct radiative forcing and its uncertainty constrained by observations, *J. Geophys. Res. Atmos.*, *121*, 5948-5971.

Kinne, S., D. O'Donnel, P. Stier, S. Kloster, K. Zhang, H. Schmidt, S. Rast, M. Giorgetta, T. F. Eck, and B. Stevens (2013), MAC-v1: A new global aerosol climatology for climate studies, *J. Adv. Model. Earth Syst.*, *5*, 704-740, doi:10.1002/jame.20035.

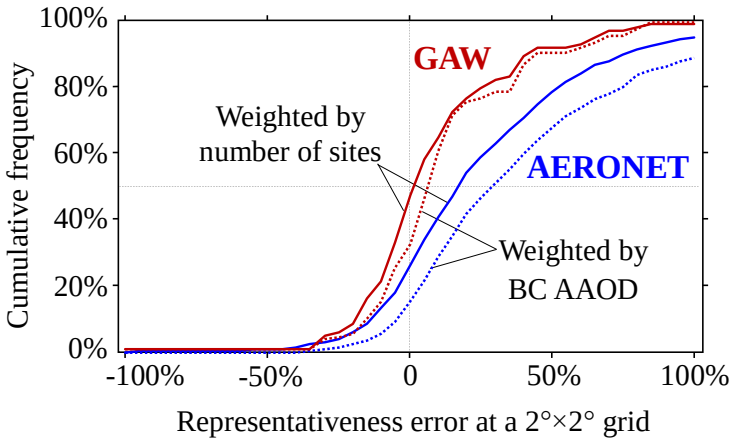

Figure S7. Evaluation of the representativeness error for the AERONET and GAW networks sensitivity tests using the 1383 AERONET sites in 2017. Cumulative frequency distributions of the representativeness error using BC AAOD over a 2°×2° grid-box relative to a 0.1°×0.1° resolution positioned at measurement sites are compared between GAW (red) and AERONET (blue). This figure is the same as **Figure 1C** in the main text, but using the 1383 AERONET sites in **Figure S4E**.

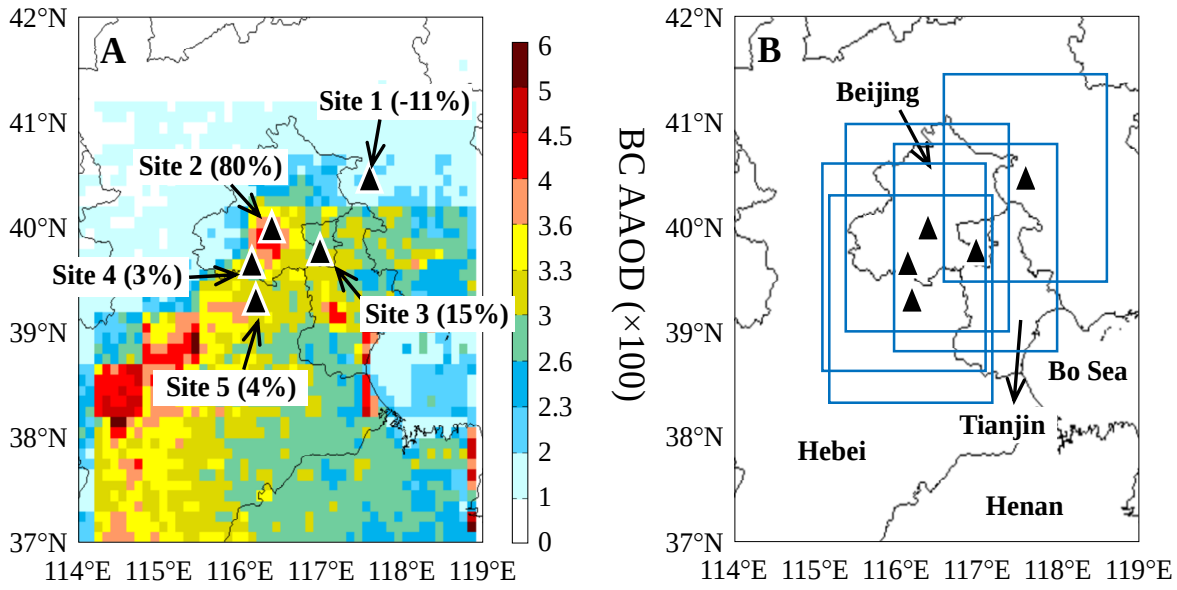

Figure S8. (A) An example of how the representativeness error depends on the location of the site. We select five AERONET sites located in the North China Plain (NCP). The downscaled BC AAOD at a resolution of 0.1°×0.1° is shown by the colorbar, and the representativeness error for each AERONET site is given in parentheses. Among the five sites, Site 2 is located in the center of Beijing. The values of BC AAOD over the 0.1°×0.1° grid-box and the 2°×2° grid-box with the AERONET sites in the grid-box center are: Site 1 (C_{fine}=0.0185; C_{coarse}=0.0207); Site 2 (C_{fine}=0.0450; C_{coarse}=0.0250); Site 3 (C_{fine}=0.0316; C_{coarse}=0.0274); Site 4 (C_{fine}=0.0288; C_{coarse}=0.0279); Site 5 (C_{fine}=0.0308; C_{coarse}=0.0296). (**B**) We show the 2°×2° grid-boxes with the five AERONET sites in the grid-box center (blue panels). The boundaries for Beijing, Tianjin, Bo Sea, Hebei and Henan Province are shown as black lines.

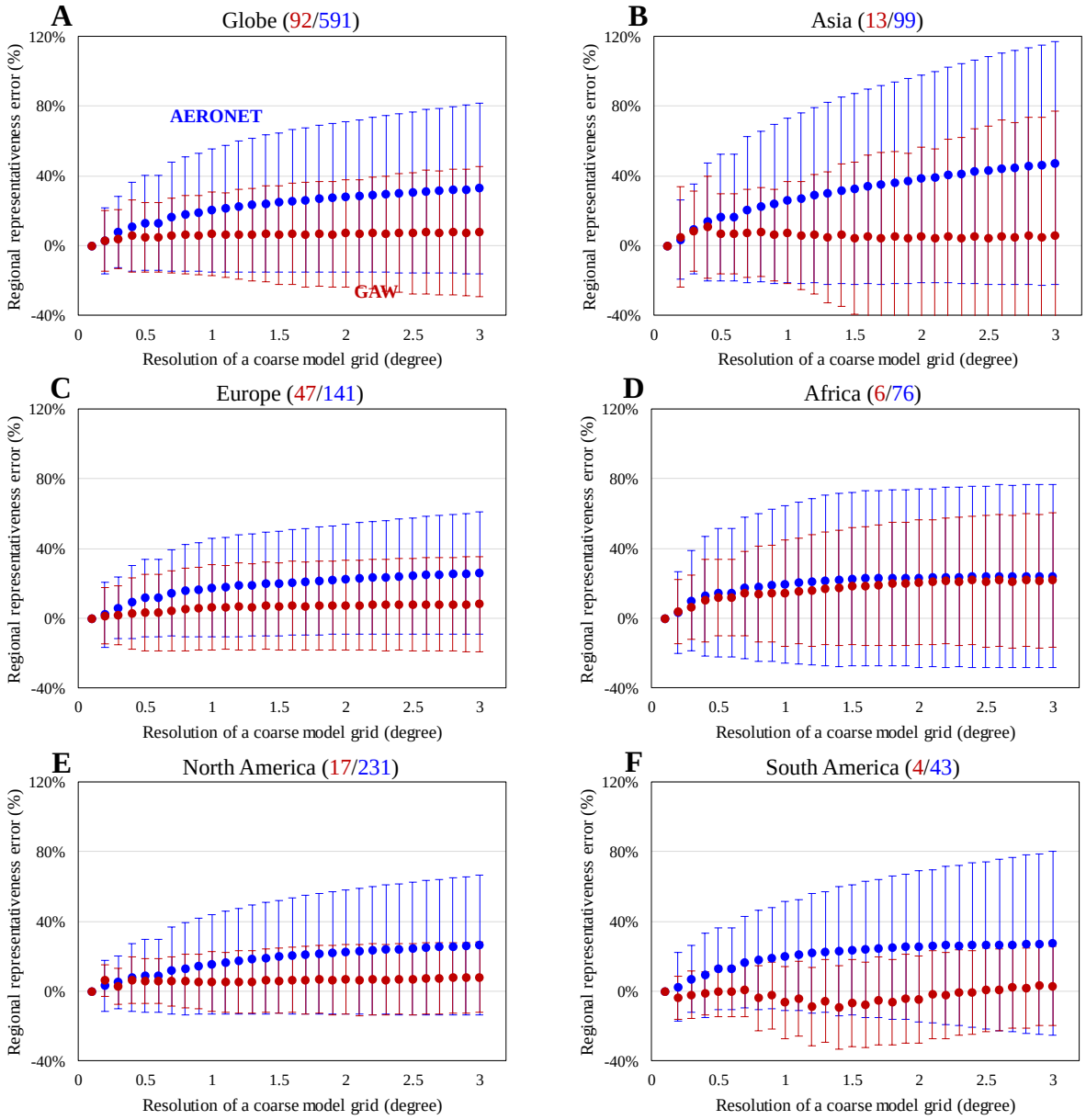

Figure S9. Dependence of the regional representativeness error on the grid resolution for sites by region in the GAW (red) and AERONET (blue) networks. (**A**) Globe; (**B**) Asia; (**C**) Europe; (**D**) Africa; (**E**) North America; and (**F**) South America. The number of sites in the GAW (red) and AERONET (blue) networks is listed in parentheses. We approximate the BC AAOD at a local site by the value of the 0.1°×0.1° grid-box it belongs to, namely C_{fine}. We define the BC AAOD over a coarse grid-box of $g°\times g°$, namely C_{coarse}, as the average over $n=(10g)^2$ 0.1°×0.1° grid-boxes with the monitoring site closest to the center. The circles in each panel of **Figure S9** show the regional representativeness error (*RRE*), defined as $RRE=(\overline{C_{fine}}-\overline{C_{coarse}})/\overline{C_{coarse}}$ for each region, where $\overline{C_{fine}}$ and $\overline{C_{coarse}}$ are the average C_{fine} and C_{coarse} for all sites in each region. The error bars in each panel of **Figure S9** show the standard deviations of representativeness errors (*RE*), defined as $RE=(C_{fine}-C_{coarse})/C_{coarse}$, for all sites in each region.